

Pseudo-one-dimensional ribbon chain cluster realized under high pressure in $1T$ -VSe₂T. Hara ¹, N. Katayama ^{1,*}, S. Kitou ², K. Kojima ³, S. Kawaguchi,⁴ and H. Sawa ¹¹*Department of Applied Physics, Nagoya University, Nagoya 464-8603, Japan*²*Department of Advanced Materials Science, University of Tokyo, Kashiwa 277-8561, Japan*³*Institute for Solid State Physics, University of Tokyo, Kashiwa 277-8561, Japan*⁴*Japan Synchrotron Radiation Research Institute (JASRI), SPring-8, Hyogo 679-5198, Japan*

(Received 22 April 2024; revised 27 June 2024; accepted 9 July 2024; published 26 July 2024)

We present a high-pressure single-crystal x-ray structure analysis of two-dimensional layered $1T$ -VSe₂, which is known to undergo an incommensurate charge density wave transition at 110 K at ambient pressure. When pressure is applied to $1T$ -VSe₂ at 150 K, a structural phase transition appears at about 8 GPa. The structural analysis of x-ray diffraction data obtained from a single crystal sample, with the correct corrections for the use of a diamond anvil cell and taking into account the effects of multiple domains, using only the superlattice peaks, reveals the appearance of “ribbon chain” type vanadium clusters at a high-pressure region. The formation of Se-Se bonds under high pressure and the associated unexpected charge injection into vanadium are largely responsible for the formation of ribbon-chain clusters. We discuss the possibility that such interanion bond formation occurs universally in the high-pressure phase of transition metal diselenides.

DOI: [10.1103/PhysRevB.110.L020103](https://doi.org/10.1103/PhysRevB.110.L020103)

As exemplified by cuprates, where high-temperature superconductivity appears when electrons and holes are doped, controlling the amount of carriers is the key to achieving novel electronic properties in condensed solids [1,2]. Chemical substitution, intercalation, and electric field effects are commonly used to control the amount of carriers, but the formation and breaking of bonds between anions formed in crystals is also useful as an effective method of controlling the amount of carriers. For example, in BaFe₂As₂ and SrFe₂As₂, the parent SDW phase is suppressed under pressure, resulting in high-temperature superconductivity [3–6], while in CaFe₂As₂ no bulk superconductivity occurs even under pressure [7]. This is due to a “volume collapsed tetragonal transition” in CaFe₂As₂, in which bonds are formed between neighboring As-As across the van der Waals gap between the layers under pressure [8]. This bond formation results in a change in the As valence to a smaller value and a significant change in the d band and spin state of the Fe sites [9]. If such bond formation and breaking chemistry can be realized on a frustrated lattice, we can expect the emergence of a wide variety of physical properties due to the charge degrees of freedom.

Such studies can be realized in layered transition metal dichalcogenides $1T$ -MX₂ (M : transition metal; X : O, S, Se, Te) in which the transition metal M has a two-dimensional triangular lattice. When $X = \text{Te}$, anionic bonds can form between neighboring Te ions, thus causing unexpected charge degrees of freedom in M . For example, $1T$ -IrTe₂ exhibits an Ir³⁺/Ir⁴⁺ charge ordering at low temperatures, forming a dimer between neighboring Ir⁴⁺ ions [10,11]. When this dimer state is suppressed by Pt doping, superconductivity

appears [12]. In $1T$ -MTe₂ ($M = \text{V, Nb, Ta}$), quasi-one-dimensional clusters called “ribbon chains” are formed [13–15], as shown in Fig. 1, due to the unexpected charge degrees of freedom arising from anionic bonds. The carrier supply from the anion brings the electronic state of M closer to $3.67+$ ($d^{4/3}$), with each M supplying $2/3$ electrons each to two linear trimer states [16]. As a result, the ribbon chain can be understood to be composed of several linear trimers formed by three-center, two-electron bonds. As in the CaFe₂As₂ example, bond formation between anions is more likely to occur as the interatomic distance shrinks under pressure. Thus, even in MX₂ compounds that do not have anion formation at ambient pressure, pressure application may induce bond formation between anions and realize various electronic properties due to unexpected charge degrees of freedom. Such pressure-based control of the number of electrons through valence engineering, combined with increased dimensionality and enhanced interactions due to pressure effects, will lead to an expansion of the field of physical property exploration.

In this paper, we report the synchrotron x-ray structural analysis of $1T$ -VSe₂. $1T$ -VSe₂ is known to exhibit a unique incommensurate charge density wave (ICDW) transition at about 110 K [17,18]. It has been shown that a structural phase transition occurs at room temperature at pressures of about 15 GPa [19–22]. Although theoretical models of the high-pressure phase and structural analysis by powder x-ray diffraction have been reported, it has been required to clarify the high-pressure structure from precise structural analysis including superlattice peaks using single crystals. Our structural analysis using superlattice peaks obtained by single-crystal XRD experiments revealed that quasi-one-dimensional clusters called “ribbon chains” appearing in $1T$ -MTe₂ ($M = \text{V, Nb, Ta}$) are realized under pressure of $1T$ -VSe₂. We argue that the contraction of the c -axis length observed with the

*Contact author: katayama.naoyuki.m5@f.mail.nagoya-u.ac.jp

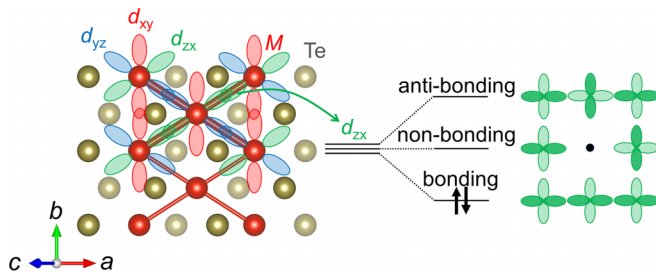


FIG. 1. Schematic picture of ribbon chain clusters appearing at ambient pressure in $1T$ - $M\text{Te}_2$ ($M = \text{V}, \text{Nb}, \text{Ta}$), with axes from monoclinic structure. In these tellurides, the M valence approaches $3.67+$ ($d^{4/3}$) with Te-Te bonding between layers. The ribbon chain consists of linear trimers connected by d orbitals, and the trimers are formed by three-center, two-electron bonds. In this paper, we show that a similar ribbon chain cluster is realized at high pressure of $1T$ - VSe_2 .

structural phase transition under pressure indicates the formation of bonds between neighboring Se ions across the van der Waals gap, with the unexpected change of a V valence and the associated ribbon chain formation. This indicates that layered MX_2 compounds are an attractive playground for the study of various electronic properties originating from the bond formation between anions and the accompanying charge degrees of freedom that appear under high pressure.

$1T$ - VSe_2 single crystals were synthesized by a conventional solid state reaction method. The mixture of the constituent elements in their stoichiometric ratios was vacuum-sealed and sintered at 500°C for 24 h and at 800°C for 72 h. The obtained samples contain tiny single crystals. The quality of the crystals was confirmed by single-crystal XRD experiments at BL02B1 beamline of SPring-8, where 2D semiconductor detector PILATUS 3X CdTe (DECTRIS Ltd, Switzerland) is equipped. Single crystals with dimensions of $30 \times 30 \times 20 \mu\text{m}^3$ were used. A He-gas blowing device was employed to cool the sample to 45 K and x-rays of $E = 40 \text{ keV}$ were used. XRD measurements under pressure were performed at the BL10XU beamline of SPring-8 [23], where a 2D imaging plate (IP) is equipped. A diamond anvil cell (DAC) apparatus was used for the experiments under pressure and a single crystal of $1T$ - VSe_2 was loaded into a stainless steel gasket hole ($230 \mu\text{m}$ in diameter) together with ruby for pressure calibration [24] and helium as pressure medium. X rays of $E = 30 \text{ keV}$ were used with a beam diameter of $40 \mu\text{m}$. A refrigerator was used for controlling temperatures and a helium gas membrane system was used for pressurization. Original software was used for extracting the peak intensity [25]. Diffraction intensity averaging and refinement of structural parameters were performed using SORTAV [26], and SHELX [27], respectively. Powder x-ray diffraction experiments of $1T$ - VTe_2 , whose synthesis was reported in a previous study [15], were performed on BL5S2 at Aichi Synchrotron Radiation Center. The measurement temperatures were 300 K and 500 K and x-rays of 18 keV were used. Crystal structure was visualized using VESTA [28].

Figure 2(a) shows the sharp Bragg peaks appearing in the single-crystal diffraction pattern of $1T$ - VSe_2 obtained in the high-temperature phase of 300 K at ambient pressure. The

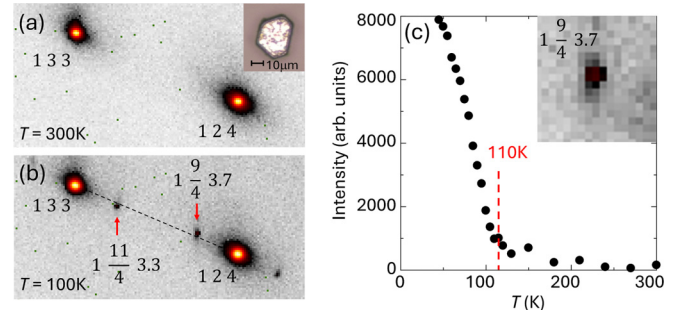


FIG. 2. (a) Part of the diffraction pattern at 300 K at ambient pressure. Inset: the single crystal of $1T$ - VSe_2 used in the XRD experiment with a diamond-anvil cell. (b) Part of the diffraction pattern at ambient pressure 100 K. (c) Temperature dependence of superlattice peak intensity at $1 \frac{9}{4} 3.7$. Inset: diffraction image around $1 \frac{9}{4} 3.7$ peak at 100 K.

inset of Fig. 2(a) shows a hexagonal platelike single crystal corresponding to the trigonal crystal structure. The data obtained at 300 K can be analyzed assuming the previously reported space group $P\bar{3}m1$ and $R_1(I > 3\sigma)$, which indicates the reliability of the analysis is 2.01%. The structural analysis shows a merohedral domain with a mirror plane perpendicular to the $a - b$ direction, as described in the Supplemental Material [29]. In the high-pressure diffraction experiments shown later, we used a high quality sample in which this ratio is so small [0.49(13)%] that it can be regarded as a single domain. When the temperature was lowered to below 110 K, superlattice peaks appeared as shown in Fig. 2(b) and their intensity increased with decreasing temperature as shown in Fig. 2(c). This temperature is consistent with the previously reported ICDW transition temperature [30], indicating the high quality of the present sample. The superlattice peaks appear at positions that are not divisible by integer exponents, consistent with the low-temperature phase being an ICDW phase with a nesting vector of $4a \times 4a \times 3.18c$ [17,18,31–33].

Figure 3(a) shows one of the single-crystal XRD images obtained at 150 K and 5.53 GPa, where no structural phase transition was observed. Importantly, in high-pressure experiments, the narrow aperture angle of the DAC and the small amplitude of the rotation method make it impossible to obtain as many diffraction peaks as in conventional experiments. Furthermore, peaks that overlapped with diffraction peaks from diamond should be excluded. Therefore, it is generally difficult to conduct accurate structural analysis with high completeness and redundancy as in conventional single-crystal XRD experiments. Although the completeness of the present data was only about 35.7%, the structure was successfully obtained with a reliability of about 4.97% for the $R_1(I > 3\sigma)$ value assuming the space group $P\bar{3}m1$ as in the structure at 300 K at ambient pressure. The details of the structural analysis are described in the Supplemental Material [29].

When the pressure was further applied, a change in the diffraction pattern occurred at 8.65 GPa. This is comparable to the transition pressure at 150 K identified in previous studies [19]. A plot of the temperature and pressure points of this study compared to the previous study [19] is shown in the

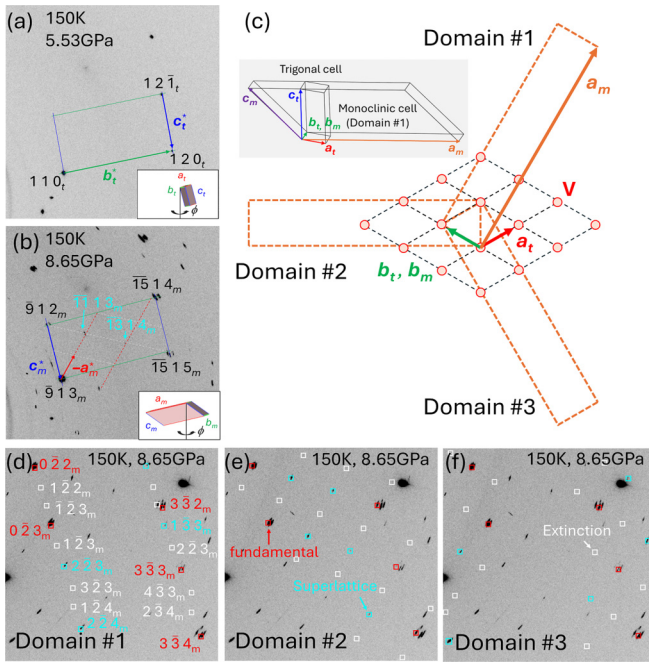


FIG. 3. (a) Part of a diffraction image measured at 150 K and 5.53 GPa. (b) Part of a diffraction image measured at 150 K and 8.65 GPa. The subscripts “*t*” and “*m*” attached to the *hkl* index indicate the indices of the trigonal unit cell at ambient pressure and the monoclinic cell at high pressure, respectively. The unit cell showing the crystal orientation corresponding to each image is shown in the inset. (c) Unit cells and orientation of the three domains appearing at 8.65 GPa. The relationship to the unit cell at ambient pressure is also shown. (d)–(f) Indexing to three domains appearing at 150 K and 8.65 GPa for each domain with monoclinic unit cells (red: fundamental peaks; blue: superlattice peaks; white: extinct peaks due to the *C*-base center lattice).

Supplemental Material [29]. Figure 3(b) shows a single-crystal XRD image obtained at 150 K and 8.65 GPa. The presence of newly emerged superlattice peaks and the splitting of existing Bragg peaks are important features. There is no extinction rule in the space group of $P\bar{3}m1$ in the high-temperature phase at ambient pressure. Therefore, the appearance of a new peak at high pressure indicates a conversion to a unit cell with a larger volume under high pressure.

The Bragg peak in the fundamental reflection split into multiple peaks with different *d* values. This indicates a symmetry lowering under high pressure and the associated emergence of domains. By assuming three domains with monoclinic unit cells with $a_m = 17.100(3)$ Å, $b_m = 3.248(3)$ Å, $c_m = 8.002(3)$ Å, and $\beta = 135.753(2)^\circ$, we could index all peaks, as shown in Figs. 3(d)–3(f). Here, the relationship between the ambient pressure phase cell (*a*, *b*, *c*) and the high-pressure phase cell (a_m , b_m , c_m) is as follows: $a_m = -3a - 6b$, $b_m = a$, and $c_m = a + 2b + c$. The three domains indexed in this study are named Domain 1, Domain 2, and Domain 3, as shown in Fig. 3(c). It should be mentioned that, in principle, six domains could emerge when lower symmetrization occurs from trigonal to monoclinic in the present structure. This would mean that three domains did not appear in the present sample or that the volume fractions were so small that they

could not be observed as peaks. The three domains and the three that were not observed are detailed in the Supplemental Material [29]. No peaks appear in the indexes indicated by the white boxes in any of the domains, as shown in Figs. 3(d)–3(f), indicating the existence of an extinction rule originating from the symmetry of the *C*-base center lattice. It is also important to note that, while the fundamental peaks appear with strong overlap, the superlattice peaks appear at different positions in each domain and do not overlap like the fundamental peaks, as clearly shown in Figs. 3(d)–3(f). This indicates that only single-domain components can be extracted with high accuracy for the superlattice peak. For the extraction of the peak intensities, we used original software that we have developed [25] to accommodate Debye elongated peak shapes due to pressure application.

For Domain 3, which has better agreement in equivalent reflection intensities, structural analysis was performed using only the intensity of superlattice reflections. Monoclinic crystals with *C*-base center lattice have space groups such as $C2$, Cm , and $C2/m$, and previous studies have proposed the $C2/m$ space group [19]. In this study, $C2/m$ was assumed following the previous study. In the $C2/m$ space group, there are two *V* sites and three Se sites in the unit cell. Since the number of observed reflections is small due to the use of DAC, we established a restraint that makes each parameter that constitutes the anisotropic temperature factor common for each of the two *V* sites and three Se sites. Using this restraint, there are a total of 17 refined parameters based on the symmetry of each element site: eight for the atomic position parameter, eight for the anisotropic temperature factor parameter, and one for the scale factor. All of these parameters were refined simultaneously and all parameters converged properly. The number of peaks used in the analysis was 93 and the $R_1(I > 3\sigma)$ value was 6.3%, a relatively good result. In this analysis, the crystal structure obtained at 5.53 GPa and 150 K in the ambient pressure phase was reconstructed into a monoclinic unit cell and used as the initial structure.

At first glance, the crystal structure obtained from the analysis resembles the ribbon chain structure of $1T-MTe_2$ ($M = V, Nb, Ta$), as shown in Fig. 1. Figure 4(a) shows a superposition of the structure of $1T-VTe_2$ at 300 K and the crystal structure of $1T-VSe_2$ at 150 K and 8.65 GPa. Since the lattice constants of the two structures are very different, the lattice constants were made artificially identical. This allows Fig. 4(a) to visually show the coincidence of the fractional coordinates of each site of the two structures. These two structures are almost perfectly identical, even though the fractional coordinates of each site in the low-temperature phase structure of $1T-VTe_2$ were not taken as initial values for the present refinement. This indicates that the results of the present analysis are reliable and clearly shows that ribbon chains occur in $1T-VSe_2$ under high pressure.

The change of cell volume and lattice constants ratio *c/a* at 150 K with pressure application is shown in Fig. 4(b). As previously reported [19,34], the decrease in cell volume becomes smaller as pressure is applied up to 8 GPa. This is due to the strong compression of the van der Waals gap, followed by the strong Coulomb repulsion between neighboring Se-Se across the van der Waals gap. Above 8 GPa, where ribbon chains are formed, the interlayer distance shortens due to Se-

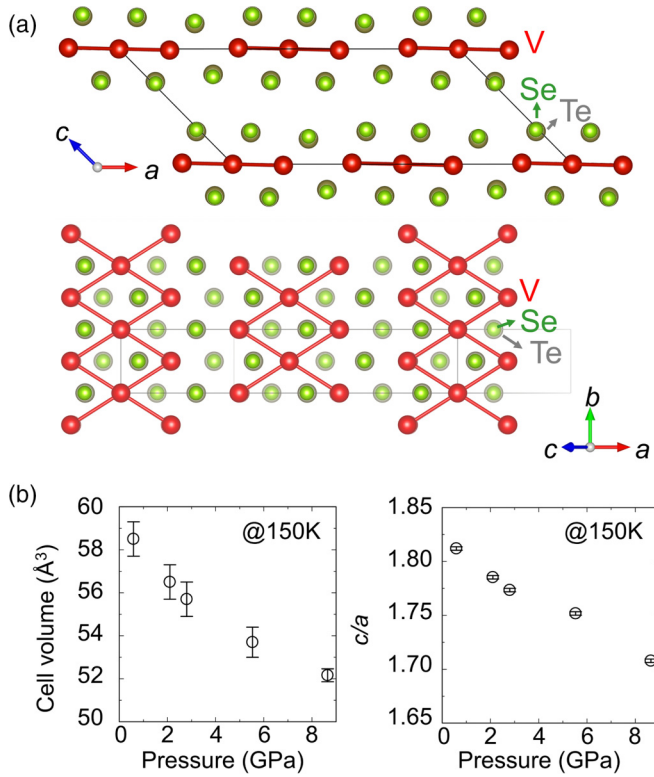


FIG. 4. (a) Superposition of the crystal structure of $1T$ -VSe₂ at 150 K and 8.65 GPa and that of $1T$ -VTe₂ at 300 K and ambient pressure. The structural parameters of $1T$ -VTe₂ are given in Ref. [15] and the unit cell is modified for comparison with $1T$ -VSe₂. The lattice constants of $1T$ -VSe₂ are adjusted so that the unit cells are the same. The V fractional coordinates are nearly equal in both structures and overlap well. (b) Pressure dependence of lattice parameters at 150 K.

Se bonding and c/a decreases suddenly. Structural analysis shows that the nearest Se-Se distance between adjacent VSe₂ layers is 3.233(4) Å at 150 K and 8.65 GPa and 3.04(4) Å at 150 K and 8.65 GPa, indicating that the Se-Se distance changes by about 5% with phase transition. These values are comparable to the powder structure analysis results of previous studies [19,21]. In $1T$ -VTe₂, which forms ribbon chains at room temperature, it is known that the Te-Te bond is broken at 480 K with increasing temperature and the ribbon chains disappear. The change in the Te-Te distance associated with this phase transition should provide a good reference for verifying the validity of the present results. Therefore, x-ray diffraction experiments of $1T$ -VTe₂ were performed at 500 K and 300 K under ambient pressure. The nearest-neighbor Te-Te distances between adjacent VTe₂ layers were 3.799(7) Å and 3.59(3) Å, respectively, indicating that the anion distance changed approximately 5% with the phase transition. Details of the analysis are given in the Supplemental Material [29]. The fact that the rate of change of the interanion distance is similar for both materials confirms the validity of the results of this $1T$ -VSe₂ pressure experiment. This Se-Se bond formation changes the valence of $1T$ -VSe₂ to $V^{(4-2\delta)+}(Se_2)^{2(2-\delta)-}$, which is closer to $V^{3.67+}$ ($d^{4/3}$) suitable for ribbon chain formation. In other words, it can be concluded that, in $1T$ -VSe₂,

a bond is formed between adjacent Se-Se across the van der Waals gap due to the application of pressure and a ribbon chain is formed in the plane as a result of carriers being supplied from Se to V.

The key factors that generate bonding between anions are the ionic radii of the anions and the distance between neighboring anions across the van der Waals gap. In $1T$ -IrTe₂ and $1T$ -MTe₂ ($M = V, Nb, Ta$), Te-Te bonds are stably formed at ambient pressure due to the large ionic radius of Te [11,15]. On the other hand, in $1T$ -VSe₂, the ionic radius of Se is smaller than that of Te, so the formation of the Se-Se bond requires pressure support. In $1T$ -CrSe₂, the Se-Se bond is formed at low temperatures without the application of pressure, probably because Cr⁴⁺ is unstable with an unusually high valence and the carrier supply associated with the formation of the Se-Se bond greatly stabilizes the energy of the electronic system [35]. Thus $1T$ -MSe₂ has an instability toward bond formation between anions, indicating that pressure application can induce bond formation between anions and a corresponding change in the electronic state of the M element, leading to a variety of electronic properties due to unexpected charge degrees of freedom.

Although the degree of freedom of charge does not seem to be important in highly itinerant materials, in two-dimensional triangular lattice systems with $1T$ structure, tuning the amount of charge dramatically changes the physical properties. For example, in Na_{*x*}CoO₂, controlling the Na amount x leads to the realization of thermoelectric semiconductors with large thermoelectric power [36], novel charge ordered states [37], and superconductivity [38] in the process changing from Co³⁺ to Co⁴⁺. In Li_{*x*}VS₂, various electronic phases are reported to be realized by controlling the Li amount x , such as ICDW in $1T$ -VS₂ [39], ribbon chain state in Li_{0.33}VS₂ [40], and metal-trimer insulating transition in LiVS₂ [41–43]. In particular, it is important to note that the ribbon chain appears at Li_{0.33}VS₂. In Li_{0.33}VS₂, the ionic radius of S is small and the S-S distance is separated by interlayer Li, so that no bond formation occurs between neighboring anions. However, the valence of V^{3.67+} is realized because the interlayer Li provides carriers. The fact that ribbon-chain clusters similar to those in the high-pressure phase of $1T$ -VSe₂ appear at low temperatures in Li_{0.33}VS₂, where the V^{3.67+} valence state is clearly guaranteed, confirms that the valence of V does indeed change under high pressure in $1T$ -VSe₂. Thus it is possible to develop various physical properties in triangular lattice compounds with the $1T$ structure by introducing charge degrees of freedom even in itinerant materials. The pressure-induced formation of chemical bonds between anions and the accompanying control of electron number may enable the emergence of new electronic properties, such as superconductivity.

Finally, we would like to discuss that, in the present $1T$ -VSe₂, a superconducting phase appears above 15 GPa [20] and a phase transition from a ribbon-chain structure to a different structure occurs above 35 GPa [34]. Although we have not been able to access these pressure regions, the effects of pressure-induced increase in dimensionality of the electronic structure [44,45] and/or unexpected interlayer interactions [38,46–48] may trigger the further structural phase transitions. Alternatively, the strengthening of Se-Se bonds under pressure may further increase the amount of charge transfer

from Se to V, achieving a carrier amount favorable to superconductivity, as in the case of the hydrate $\text{Na}_x\text{CoO}_2\cdot y\text{H}_2\text{O}$. If we can establish a methodology to freely control the charge tuning technique produced under pressure found in this study in combination with these other pressure effects, it should open the way for further exploration of physical properties.

The authors are grateful to N. Hirao for the experimental support. The work leading to these results has received funding from JSPS KAKENHI (Grants No. JP20H02604, No. JP21K18599, No. JP23H04104, No. JP24H01620, and No. JP24K01329) and Thermal and Electric Energy Technology Inc. Foundation. One of the au-

thors, T.H., would like to take this opportunity to thank the Nagoya University Interdisciplinary Frontier Fellowship supported by Nagoya University and JST, the establishment of university fellowships toward the creation of science technology innovation, Grant No. JPMJF2120. Single crystal synchrotron XRD experiment under high pressure was performed at BL10XU (Proposal No. 2020A0663) and single crystal synchrotron XRD experiment under ambient pressure was performed at BL02B1 (Proposals No. 2020A0663 and No. 2019A0070-2021A0070), equipped at SPring-8, Hyogo, Japan. Powder x-ray diffraction experiments were performed on BL5S2 at Aichi SR (Proposals No. 202202037, No. 202201033, No. 202105170, and No. 202104111).

- [1] J. B. Torrance, Y. Tokura, A. I. Nazzari, A. Bezinge, T. C. Huang, and S. S. P. Parkin, Anomalous disappearance of high- T_c superconductivity at high hole concentration in metallic $\text{La}_{2-x}\text{Sr}_x\text{CuO}_4$, *Phys. Rev. Lett.* **61**, 1127 (1988).
- [2] H. Takagi, T. Ido, S. Ishibashi, M. Uota, S. Uchida, and Y. Tokura, Superconductor-to-nonsuperconductor transition in $(\text{La}_{1-x}\text{Sr})_2\text{CuO}_4$ as investigated by transport and magnetic measurements, *Phys. Rev. B* **40**, 2254 (1989).
- [3] K. Kitagawa, N. Katayama, K. Ohgushi, M. Yoshida, and M. Takigawa, Commensurate itinerant antiferromagnetism in BaFe_2As_2 : ^{75}As -NMR studies on a self-flux grown single crystal, *J. Phys. Soc. Jpn.* **77**, 114709 (2008).
- [4] K. Matsubayashi, N. Katayama, K. Ohgushi, A. Yamada, K. Munakata, T. Matsumoto, and Y. Uwatoko, Intrinsic properties of AFe_2As_2 ($\text{A} = \text{Ba}, \text{Sr}$) single crystal under highly hydrostatic pressure conditions, *J. Phys. Soc. Jpn.* **78**, 073706 (2009).
- [5] K. Kitagawa, N. Katayama, K. Ohgushi, and M. Takigawa, Antiferromagnetism of SrFe_2As_2 studied by single-crystal ^{75}As -NMR, *J. Phys. Soc. Jpn.* **78**, 063706 (2009).
- [6] K. Kitagawa, N. Katayama, H. Gotou, T. Yagi, K. Ohgushi, T. Matsumoto, Y. Uwatoko, and M. Takigawa, Spontaneous formation of a superconducting and antiferromagnetic hybrid state in SrFe_2As_2 under high pressure, *Phys. Rev. Lett.* **103**, 257002 (2009).
- [7] W. Yu, A. A. Aczel, T. J. Williams, S. L. Budko, N. Ni, P. C. Canfield, and G. M. Luke, Absence of superconductivity in single-phase CaFe_2As_2 under hydrostatic pressure, *Phys. Rev. B* **79**, 020511(R) (2009).
- [8] A. Kreyssig, M. A. Green, Y. Lee, G. D. Samolyuk, P. Zajdel, J. W. Lynn, S. L. Bud'ko, M. S. Torikachvili, N. Ni, S. Nandi, J. B. Leao, S. J. Poulton, D. N. Argyriou, B. N. Harmon, R. J. McQueeney, P. C. Canfield, and A. I. Goldman, Pressure-induced volume-collapsed tetragonal phase of CaFe_2As_2 as seen via neutron scattering, *Phys. Rev. B* **78**, 184517 (2008).
- [9] T. Yildirim, Strong coupling of the Fe-spin state and the As-As hybridization in iron-pnictide superconductors from first-principle calculations, *Phys. Rev. Lett.* **102**, 037003 (2009).
- [10] K.-T. Ko, H.-H. Lee, D.-H. Kim, J.-J. Yang, S.-W. Cheong, M. J. Eom, J. S. Kim, R. Gammag, K.-S. Kim, H.-S. Kim, T.-H. Kim, H.-W. Yeom, T.-Y. Koo, H.-D. Kim, and J.-H. Park, Charge-ordering cascade with spin-orbit Mott dimer states in metallic iridium ditelluride, *Nat. Commun.* **6**, 7342 (2015).
- [11] T. Toriyama, M. Kobori, T. Konishi, Y. Ohta, K. Sugimoto, J. Kim, A. Fujiwara, S. Pyon, K. Kudo, and M. Nohara, Switching of conducting planes by partial dimer formation in IrTe_2 , *J. Phys. Soc. Jpn.* **83**, 033701 (2014).
- [12] S. Pyon, K. Kudo, and M. Nohara, Superconductivity induced by bond breaking in the triangular lattice of IrTe_2 , *J. Phys. Soc. Jpn.* **81**, 053701 (2012).
- [13] K. Bronsema, G. Bus, and G. Wieggers, The crystal structure of vanadium ditelluride, $\text{V}_{1+x}\text{Te}_2$, *J. Solid State Chem.* **53**, 415 (1984).
- [14] B. Brown, The crystal structures of NbTe_2 and TaTe_2 , *Acta Crystallogr.* **20**, 264 (1966).
- [15] N. Katayama, Y. Matsuda, K. Kojima, T. Hara, S. Kitou, N. Mitsuishi, H. Takahashi, S. Ishiwata, K. Ishizaka, and H. Sawa, Observation of local atomic displacements intrinsic to the double zigzag chain structure of $1T\text{-}M\text{Te}_2$ ($M = \text{V}, \text{Nb}, \text{Ta}$), *Phys. Rev. B* **107**, 245113 (2023).
- [16] M.-H. Whangbo and E. Canadell, Analogies between the concepts of molecular chemistry and solid-state physics concerning structural instabilities. Electronic origin of the structural modulations in layered transition metal dichalcogenides, *J. Am. Chem. Soc.* **114**, 9587 (1992).
- [17] K. Terashima, T. Sato, H. Komatsu, T. Takahashi, N. Maeda, and K. Hayashi, Charge-density wave transition of $1T\text{-VSe}_2$ studied by angle-resolved photoemission spectroscopy, *Phys. Rev. B* **68**, 155108 (2003).
- [18] K. Tsutsumi, X-ray-diffraction study of the periodic lattice distortion associated with a charge-density wave in $1T\text{-VSe}_2$, *Phys. Rev. B* **26**, 5756 (1982).
- [19] R. Sereika, C. Park, C. Kenney-Benson, S. Bandaru, N. J. English, Q. Yin, H. Lei, N. Chen, C. J. Sun, S. M. Heald, J. Ren, J. Chang, Y. Ding, and H. k. Mao, Novel superstructure-phase two-dimensional material $1T\text{-VSe}_2$ at high pressure, *J. Phys. Chem. Lett.* **11**, 380 (2020).
- [20] S. Sahoo, U. Dutta, L. Harnagea, A. K. Sood, and S. Karmakar, Pressure-induced suppression of charge density wave and emergence of superconductivity in $1T\text{-VSe}_2$, *Phys. Rev. B* **101**, 014514 (2020).
- [21] J. Feng, R. A. Susilo, B. Lin, W. Deng, Y. Wang, L. B., K. Jiang, Z. Chen, X. Xing, Z. Shi, C. Wang, and B. Chen,

- Achieving room-temperature charge density wave in transition metal dichalcogenide $1T$ -VSe₂, *Adv. Eletron. Mater.* **6**, 1901427 (2020).
- [22] S. Pal, K. Debnath, S. N. Gupta, L. Harnagea, D. V. S. Muthu, U. V. Waghmare, and A. K. Sood, Pressure-induced $1T$ to $3R$ structural phase transition in metallic VSe₂: X-ray diffraction and first-principles theory, *Phys. Rev. B* **104**, 014108 (2021).
- [23] N. Hirao, S. I. Kawaguchi, K. Hirose, K. Shimizu, E. Ohtani, and Y. Ohishi, New developments in high-pressure x-ray diffraction beamline for diamond anvil cell at SPring-8, *Matter Radiat. Extremes* **5**, 018403 (2020).
- [24] C.-S. Zha, H.-K. Mao, and R. Hemley, Elasticity of MgO and a primary pressure scale to 55 GPa, *Proc. Natl. Acad. Sci. USA* **97**, 13494 (2000).
- [25] K. Sugawara, K. Sugimoto, T. Fujii, T. Higuchi, N. Katayama, Y. Okamoto, and H. Sawa, Direct visualization of orbital flipping in volborthite by charge density analysis using detwinned data, *J. Phys. Soc. Jpn.* **87**, 024601 (2018).
- [26] R. Blessing, Data reduction and error analysis for accurate single crystal diffraction intensities, *Crystallogr. Rev.* **1**, 3 (1987).
- [27] G. Sheldrick, A short history of *SHELX*, *Acta Crystallogr., A* **64**, 112 (2008).
- [28] K. Momma and F. Izumi, *VESTA3* for three-dimensional visualization of crystal, volumetric and morphology data, *J. Appl. Crystallogr.* **44**, 1272 (2011).
- [29] See Supplemental Material at <http://link.aps.org/supplemental/10.1103/PhysRevB.110.L020103> for experimental details and structural aspects.
- [30] A. Toriumi and S. Tanaka, Galvanomagnetic properties of $1T$ -VSe₂, *Physica B+C* **105**, 141 (1981).
- [31] A. H. Thompson and B. G. Silbernagel, Correlated magnetic and transport properties in the charge-density-wave states of VSe₂, *Phys. Rev. B* **19**, 3420 (1979).
- [32] D. J. Eaglesham, R. L. Withers, and D. M. Bird, Charge-density-wave transitions in $1T$ -VSe₂, *J. Phys. C: Solid State Phys.* **19**, 359 (1986).
- [33] J. Pandey and A. Soni, Electron-phonon interactions and two-phonon modes associated with charge density wave in single crystalline $1T$ -VSe₂, *Phys. Rev. Res.* **2**, 033118 (2020).
- [34] D. Song, Y. Zhou, M. Zhang, X. He, and X. Li, Structural and transport properties of $1T$ -VSe₂ single crystal under high pressures, *Front. Mater.* **8**, 710849 (2021).
- [35] S. Kobayashi, N. Katayama, T. Manjo, H. Ueda, C. Michioka, J. Sugiyama, Y. Sassa, O. K. Forslund, M. Månsson, K. Yoshimura, and H. Sawa, Linear trimer formation with antiferromagnetic ordering in $1T$ -CrSe₂ originating from Peierls-like instabilities and interlayer Se-Se interactions, *Inorg. Chem.* **58**, 14304 (2019).
- [36] I. Terasaki, Y. Sasago, and K. Uchinokura, Large thermoelectric power in NaCo₂O₄ single crystals, *Phys. Rev. B* **56**, R12685 (1997).
- [37] H. Yang, R. Xiao, C. Ma, H. Tian, D. Wu, and J. Li, Charge and orbital ordering in Na_{0.5}CoO₂, *Solid State Commun.* **142**, 718 (2007).
- [38] K. Takada, H. Sakurai, E. Takayama-Muromachi, F. Izumi, R. A. Dilanian, and T. Sasaki, Superconductivity in two-dimensional CoO₂ layers, *Nature (London)* **422**, 53 (2003).
- [39] M. Mulazzi, A. Chainani, N. Katayama, R. Eguchi, M. Matsunami, H. Ohashi, Y. Senba, M. Nohara, M. Uchida, H. Takagi, and S. Shin, Absence of nesting in the charge-density-wave system $1T$ -VS₂ as seen by photoelectron spectroscopy, *Phys. Rev. B* **82**, 075130 (2010).
- [40] N. Katayama, S. Tamura, T. Yamaguchi, K. Sugimoto, K. Iida, T. Matsukawa, A. Hoshikawa, T. Ishigaki, S. Kobayashi, Y. Ohta, and H. Sawa, Large entropy change derived from orbitally assisted three-centered two-electron σ bond formation in metallic Li_{0.33}VS₂, *Phys. Rev. B* **98**, 081104(R) (2018).
- [41] N. Katayama, M. Uchida, D. Hashizume, S. Niitaka, J. Matsuno, D. Matsumura, Y. Nishihata, J. Mizuki, N. Takeshita, A. Gauzzi, M. Nohara, and H. Takagi, Anomalous metallic state in the vicinity of metal to valence-bond solid insulator transition in LiVS₂, *Phys. Rev. Lett.* **103**, 146405 (2009).
- [42] N. Katayama, K. Kojima, T. Yamaguchi, S. Hattori, S. Tamura, K. Ohara, S. Kobayashi, K. Sugimoto, Y. Ohta, K. Saitoh, and H. Sawa, Slow dynamics of disordered zigzag chain molecules in layered LiVS₂ under electron irradiation, *npj Quantum Mater.* **6**, 16 (2021).
- [43] T. Tanaka, Y. Kawasaki, S. Endou, S. Kimura, Y. Ideta, Y. Kishimoto, T. Ohno, N. Katayama, M. Nohara, and H. Takagi, Trimer V³⁺ spin singlet state and pseudo gap in LiVS₂ studied by ⁵¹V and ⁷Li nuclear magnetic resonance, *J. Phys. Soc. Jpn.* **78**, 054709 (2009).
- [44] S. Kitou, A. Nakano, S. Kobayashi, K. Sugawara, N. Katayama, N. Maejima, A. Machida, T. Watanuki, K. Ichimura, S. Tanda, T. Nakamura, and H. Sawa, Effect of Cu intercalation and pressure on excitonic interaction in $1T$ -TiSe₂, *Phys. Rev. B* **99**, 104109 (2019).
- [45] Z. Zhao, H. Zhang, H. Yuan, S. Wang, Q. Lin, Y. Zeng, G. Xu, Z. Liu, G. K. Solanki, K. D. Patel, Y. Cui, H. Y. Hwang, and W. L. Mao, Pressure induced metallization with absence of structural transition in layered molybdenum diselenide, *Nat. Commun.* **6**, 7312 (2015).
- [46] A. Nakano, K. Sugawara, S. Tamura, N. Katayama, K. Matsubayashi, T. Okada, K. Uwatoko, Y. Munakata, A. Nakao, H. Sagayama, R. Kumai, K. Sugimoto, N. Maejima, A. Machida, T. Watanuki, and H. Sawa, Pressure-induced coherent sliding-layer transition in the excitonic insulator Ta₂NiSe₅, *IUCr J* **5**, 158 (2018).
- [47] M. A. ElGhazali, P. G. Naumov, H. Mirhosseini, V. Süß, L. MÜchler, W. Schnelle, C. Felser, and S. A. Medvedev, Pressure-induced superconductivity up to 13.1 K in the pyrite phase of palladium diselenide PdSe₂, *Phys. Rev. B* **96**, 060509(R) (2017).
- [48] K. Jiang, A. Cui, S. Shao, J. Feng, H. Dong, B. Chen, Y. Wang, Z. Hu, and J. Chu, New pressure stabilization structure in two-dimensional PtSe₂, *J. Phys. Chem. Lett.* **11**, 7342 (2020).